Materials Advances

ROYAL SOCIETY OF CHEMISTRY

PAPER

View Article Online
View Journal | View Issue

Cite this: *Mater. Adv.*, 2025, **6**, 6755

Blue emission in sterically shielded multiresonant thermally activated delayed fluorescence emitters

Mahni Fatahi, †[a] Dongyang Chen †[ab] and Eli Zysman-Colman *[a]

Multi-resonant TADF materials are a promising class of emitters capable of addressing the BT.2020 industry requirement for blue emission in electroluminescent displays as they simultaneously show narrowband emission and can harvest both singlet and triplet excitons to produce light. However, these emitters are typically planar and prone to aggregation and their moderately large singlet–triplet energy gap (ΔE_{ST}) leads to slow upconversion kinetics resulting in severe efficiency roll-off in the device. In this study we present a molecular design that simultaneously results in an emitter having a faster reverse intersystem crossing rate constant (k_{RISC}) and suppressed aggregation in the film state. **Mes-*t*DABNA** emits at λ_{PL} of 465 nm as 4 wt% doped films in SF3-RZ and has a short delayed lifetime of 45.2 μs. Vacuum-deposited OLEDs with **Mes-*t*DABNA** showed blue emission at CIE coordinates of (0.13, 0.15) and a maximum external quantum efficiency, EQE_{max}, of 18.4%. Unsurprisingly, these devices suffered from rather strong efficiency roll-off (EQE_{1000} of 5.6%). With the aim of addressing this efficiency roll-off, hyperfluorescent devices containing **DMAC-DPS** as a TADF sensitizer were fabricated, which showed an improved EQE_{max} of 23.1% at CIE coordinates of (0.13, 0.17) and milder efficiency roll-off (EQE_{1000} of 12.7%). These devices showed one of the highest EQE_{1000} based on DABNA-based emitters to date.

Received 4th June 2025,
Accepted 15th August 2025

DOI: 10.1039/d5ma00586h

rsc.li/materials-advances

Introduction

In recent years, thermally activated delayed fluorescence (TADF) emitters have emerged as one of the most promising emitter materials for organic light-emitting diodes (OLEDs). This is because of their excellent exciton harvesting properties that rival those of phosphorescent materials. TADF emitters are capable of harvesting up to 100% of the electrically generated excitons due to their small energy gap between the lowest excited singlet (S_1) and triplet excited states (T_1), ΔE_{ST}.[1] A subclass of TADF compounds, multi-resonant TADF (MR-TADF) emitters, produces desirable, bright, narrowband emission associated with high photoluminescence quantum yields ($\Phi_{PL} > 90\%$) and narrow full-width half maxima (FWHM < 50 nm). MR-TADF emitters are typically p- and n-doped polycyclic aromatic hydrocarbons (PAHs) having low-lying excited states possessing short-range charge transfer (SRCT) character.[2–7] A key challenge in emitter design, including for MR-TADF emitters, is achieving the blue Commission Internationale de l'Éclairage (CIE) coordinates of (0.131, 0.046) specified by the BT.2020 standard for pure blue emission.

However, the planar structure of most MR-TADF emitter cores makes them prone to aggregation, leading to red-shifted and broadened emission spectra, as well as aggregation-caused quenching (ACQ), all of which are detracting features that adversely affect the color and Φ_{PL} of blue MR-TADF emitters. For example, the first reported MR-TADF emitter, **DABNA-1** (Fig. 1), emits at λ_{PL} at 460 nm (FWHM = 28 nm) and has a Φ_{PL} of 88% in 1 wt% doped films in mCBP.[8] However, Lee *et al.* disclosed that serious ACQ occurred when concentrations of greater than 5 wt% of **DABNA-1** were used in doped films,[9] and peripheral bulky groups like *tert*-butyl moieties can mitigate it. The derivative ***t*-DABNA** (Fig. 1) maintains a high Φ_{PL} of 85%, and blue λ_{PL} of 464 nm at 5 wt% doping in DPEPO film. The OLEDs with 5 wt% ***t*-DABNA** in DPEPO showed a higher EQE_{max} of 25.1% at λ_{EL} of 467 nm and CIE coordinates of (0.13, 0.15) compared to the device with 5 wt% **DABNA-1** in mCBP (EQE_{max} = 12.5%; λ_{EL} of 461 nm, CIE coordinates of (0.13, 0.10)).[8] However, both devices still suffered from severe efficiency roll-off and the devices did not even reach a luminance of 1000 cd m^{-2}.[9] There have since been a number of studies focussing on addressing this issue by decorating the ***t*DABNA** core with different bulky moieties. For instance, ***t*DABNA-dtB**,[10] **DABNA-NP-TB** (also published as **3tPAB** and ***t*-DAB-DPA**),[11–13] ***t*DPAC-BN**[14] and **M-*t*DABNA**[15] are all examples with bulky substituents at the *para* position to the boron on the central phenyl ring (Fig. 1). The **DABNA** derivatives containing an electron-donating group show blue-shifted emission at λ_{PL}

[a] *Organic Semiconductor Centre, EaStCHEM School of Chemistry, University of St Andrews, St Andrews, KY16 9ST, UK*
E-mail: eli.zysman-colman@st-andrews.ac.uk
[b] *Institute of Functional Nano & Soft Materials (FUNSOM), Soochow University, Suzhou, 21523, Jiangsu, P. R. China*
† These authors contributed equally.

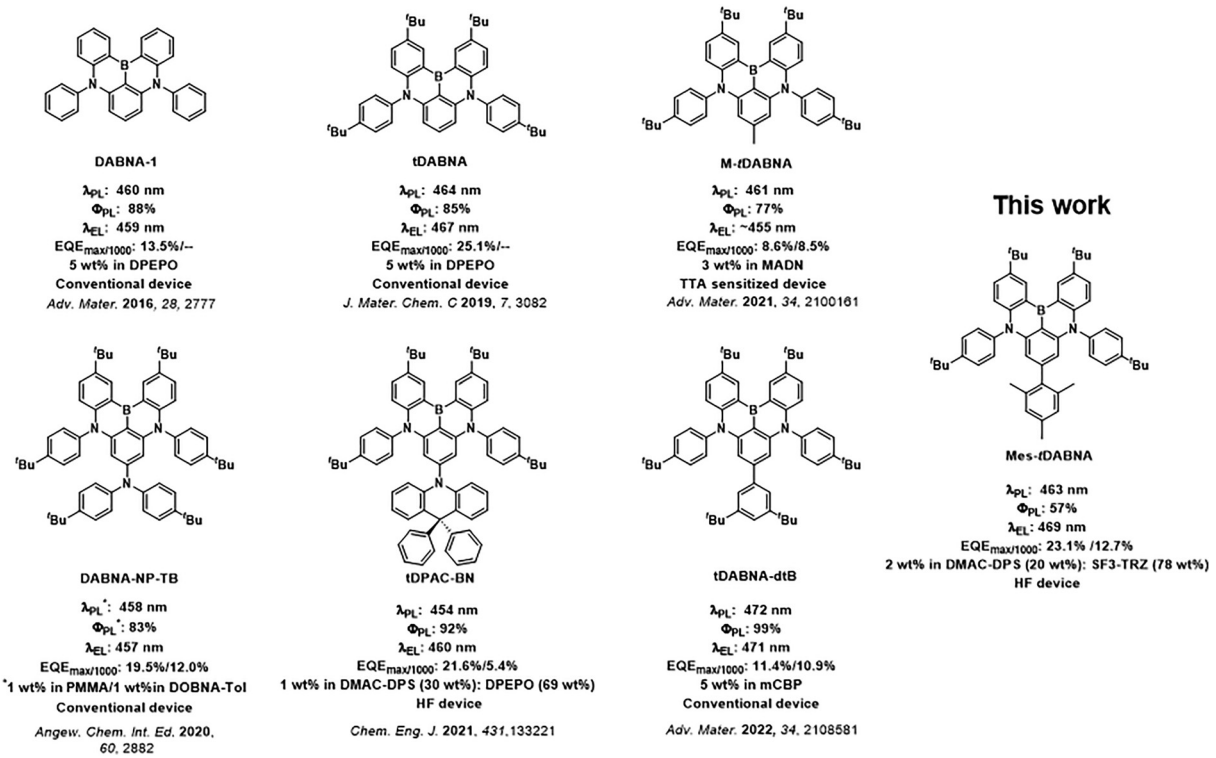

Fig. 1 Chemical structures, photophysical properties and device performance of **Mes-*t*DABNA** and examples of ***t*DABNA** derivatives in literature.[10–15]

of 461, 458, and 454 nm for **M-*t*DABNA** (3 wt% mCBP), **DABNA-NP-TB** (3 wt% *m*CP) and ***t*DPAC-BN** (1 wt% : 30 wt% **DMAc-DPS** : DPEPO), respectively, compared to ***t*DABNA** (466 nm, 3 wt% mCBP). Whereas ***t*-DABNA-dtB**, contains uses di-*tert*-butylphenyl substituent, shows a red-shifted emission to 472 nm (5 wt% mCBP), compared to ***t*DABNA** (466 nm, 3 wt% mCBP), this red shift can be explained by the larger conjugated system in this molecule. The device with 5 wt% ***t*-DABNA-dtB** showed a rather low EQE_{max} of 11.4% but also low efficiency roll-off, reflected in an EQE_{1000} of 10.9%. The lower EQE_{max} is due to the choice of device stack that is optimised for device lifetime rather than high EQE (LT_{95} = 205 h). The CIE coordinates of the device of (CIE 0.11, 0.14) are similar to those of devices with **DABNA-1**. The OLED with the donor-extended derivative ***t*DPAC-BN** showed an EQE_{max} of 21.6% at CIE coordinates of (0.14, 0.09). Similar to the devices with the aforementioned derivatives as emitters, that with ***t*DPAC-BN** showed a reduced efficiency roll-off and the EQE_{1000} was 5.4%. Devices reported by Kim *et al.* employing **DABNA-NP-TB** (***t*-DAB-DPA**) as the emitter showed a higher EQE_{max} of 27.9% [CIE coordinates of (0.13, 0.08)] as compared to that with ***t*DABNA** [23.9%; CIE coordinates of (0.13, 0.10)] accompanied by a less severe efficiency roll-off (EQE_{1000} of 8.1% as compared to 3.4% for the device with ***t*DABNA**).[11] This consistently improved performance of the OLEDs employing ***t*DABNA** derivatives as emitters compared to devices with the parent can be correlated to two factors: one is the reduced ACQ and second is the faster k_{RISC} of 3.97×10^4 s^{-1} for **DABNA-NP-TB** (***t*-DAB-DPA**) (3 wt% in mCBP:mCBPCN) *versus* 1.17×10^4 s^{-1} for ***t*DABNA** (3 wt% in mCBP:mCBPCN),[11] which reduces the likelihood of triplet quenching processes.

From these examples, a correlation between reduced efficiency roll-off and mitigated ACQ can be drawn. As previously reported by some of us, the introduction of mesityl groups onto planar MR-TADF cores can effectively reduce ACQ. One example is the decoration of three mesityl groups about the carbonyl/nitrogen based core **DiKTa** (QAO).[16] The OLEDs with **Mes3DiKTa** showed an EQE_{max} of 21.1% and an EQE_{100} of 14.5%, which represents an improved performance as compared to the device with **DiKTa** (EQE_{max} = 14.7%; EQE_{100} = 8.5%).[17]

In this study, we present a novel blue MR-TADF emitter, **Mes-*t*DABNA** (Fig. 1) that conserves the blue emission of the ***t*DABNA** core while simultaneously mitigating aggregation and alleviating efficiency roll-off in vacuum-deposited OLEDs. This is achieved by incorporating a mesityl group at the *para* position to the boron atom, which in contrast to the 3,5-di-*tert*-butyl-phenyl group used in ***t*-DABNA-dtB** does not increase the conjugation length and only serves as a steric blocking group. Theoretical calculations predict a small ΔE_{ST} of 160 meV and low-lying SRCT excited states. In toluene solution, **Mes-*t*DABNA** shows narrowband blue emission at λ_{PL} of 460 nm (FWHM of 25 nm). The emission is red-shifted to 464 nm and broadened (FWHM of 39 nm) as a 4 wt% doped film in SF3-TRZ. In these films, **Mes-*t*DABNA** has a prompt lifetime, $\tau_{p,avg}$ of 13.4 ns, and a delayed emission lifetime, $\tau_{d,avg}$, of 45 μs. This leads to a relatively faster k_{RISC} of 5.53×10^4 s^{-1} as compared to ***t*DABNA** (k_{RISC} = 2.44×10^3 s^{-1}; 5 wt% doped films in DPEPO).[9] The

OLEDs showed an EQE_{max} of 18.4% and a maximum luminance (L_{max}) of 3600 cd m^{-2}. Unfortunately, these devices showed a strong efficiency roll-off (EQE_{1000} of 5.6%), so we explored a hyperfluorescent (HF) device structure to enhance the device performance. The HF devices showed an improved EQE_{max} of 23.1% and a milder efficiency roll-off (EQE_{1000} of 12.7%). The maximum luminance was also more than doubled to 8400 cd m^{-2}.

Results and discussion

Synthesis and characterisation

The synthesis was carried out as shown in Scheme 1. Nucleophilic aromatic substitution of bis(di-*tert*-butyl)amine with bromo-4-chloro-3,5-difluorobenzene gave **2** in 43% yield. The mesityl group was installed *via* a Suzuki–Miyaura cross-coupling between mesitylboronic acid and **2** in 84% yield. Compound **3** was subjected to a tandem lithiation and borylation protocol[8] to afford **Mes-*t*DABNA** in a 21% yield, which is somewhat lower compared to those reported for **DABNA-1** (32%)[8] and ***t*DABNA** (31%)[9] but similar to that reported for **M-*t*DABNA** (27%).[15] The identity and purity of **Mes-*t*DABNA** and the intermediates were determined using melting point (Mp) analysis, ^1H and ^{13}C nuclear magnetic resonance (NMR) spectroscopy, high-resolution mass spectrometry (HRMS), high performance liquid chromatography (HPLC) and elemental analysis. Thermal gravimetric analysis (TGA) and Mp determination revealed that **Mes-*t*DABNA** has a high melting point of 300–304 °C and degradation temperature, T_d (at 5% weight loss) of 363 °C (Fig. S3), the latter of which is lower compared to that of ***t*DABNA** (419 °C).[9]

Theoretical calculations

The optimized ground-state geometry and electronic structure of **Mes-*t*DABNA** were calculated using density functional theory (DFT) at the PBE0/6-31G(d,p) level in the gas phase.[18] The HOMO is localized on the central benzene and one half of each of the amine donor moieties that is conjugated to it. Due to the symmetry of the compound, there is no electron density on either the boron atom or the *ipso* or *para* carbons to it of the central aryl ring. The electron density of the LUMO is distributed over the same skeleton as the HOMO but with significant density on boron and also the carbon centres *ipso* and *para* to it. The calculated HOMO/LUMO energy levels are −4.82/−0.94 eV. Both the HOMO and LUMO are stabilized compared to those of **M-*t*DABNA** (−4.79/−0.88 eV) (Fig. S1), which is due to the weakly inductively electron-withdrawing character of the mesityl group.

The spin–orbit coupling matrix element (SOCME) between S_1 and T_1 state at the T_1 optimized geometry calculated at the TDA-DFT-PBE0/6-31G(d,p) level of theory is not unusually small at 0.06 cm^{-1}.[19] The excited-state energies were calculated at the spin-component scaling second-order algebraic diagrammatic construction **(SCS-(ADC)2/cc-pVDZ)** level, as this level of theory has been shown to predict accurately the ΔE_{ST} of MR-TADF compounds.[20] The energy for the first excited singlet (S_1) and triplet (T_1) states are 2.91 and 2.75 eV, respectively, leading to a moderately small energy gap between (ΔE_{ST}) of 0.16 eV. Compared to **M-*t*DABNA** (3.15/3.03 eV), both the S_1 and T_1 states are stabilized while the ΔE_{ST} is larger by 40 meV. The difference

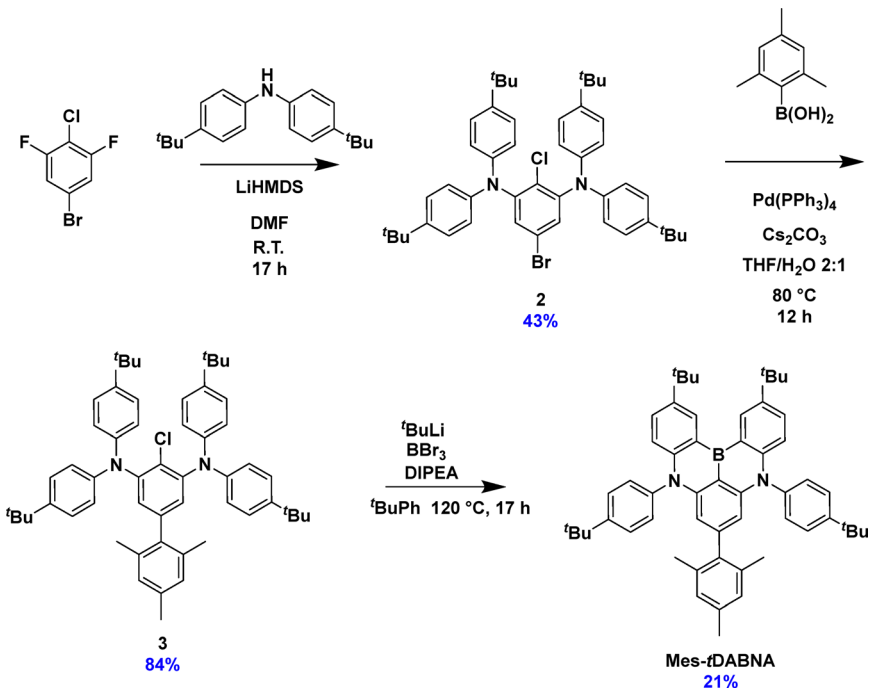

Scheme 1 Synthesis of **Mes-*t*DABNA**.

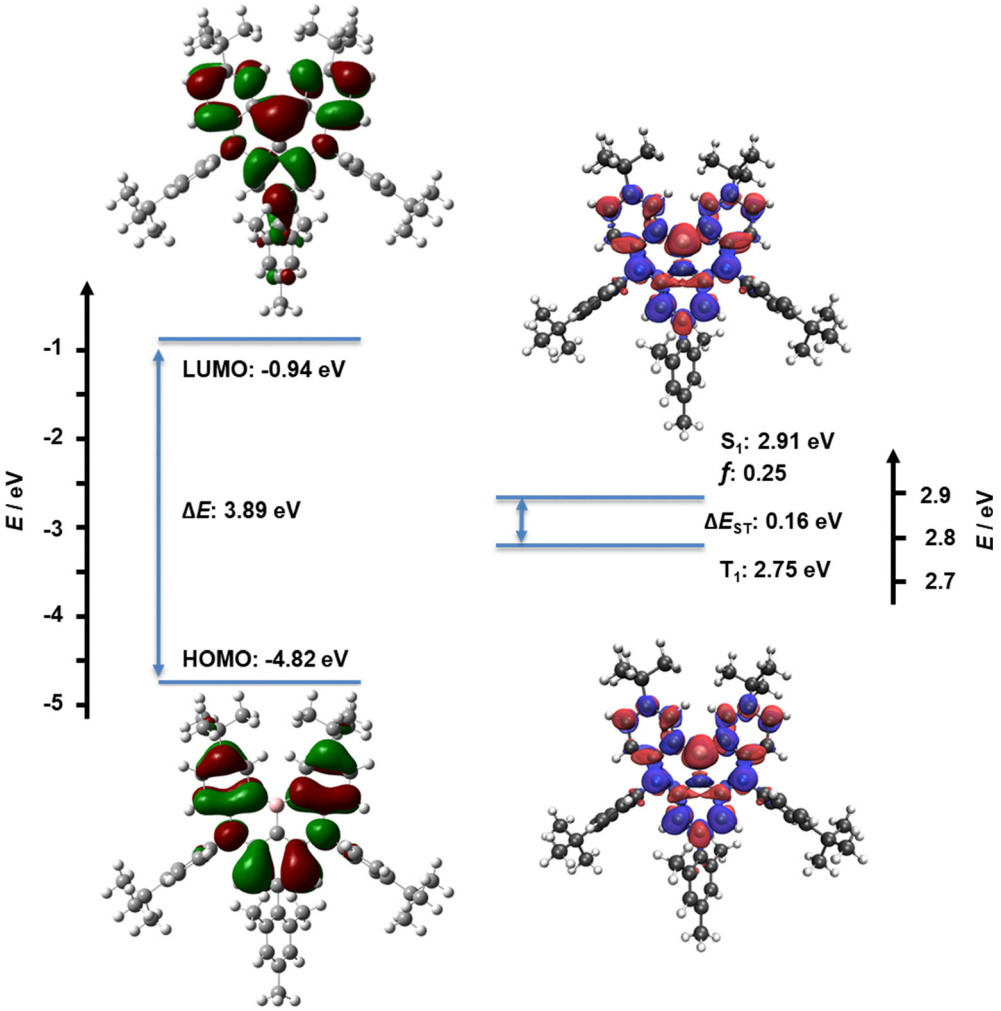

Fig. 2 Calculated HOMO and LUMO energies and the electron density plots calculated of **M-*t*DABNA** at the PBE0/6-31G(d,p) level in the gas phase and calculated excited-state energies and the corresponding difference density plots for hole and electron for the S_1 and T_1 states at the SCS-ADC(2)/cc-pVDZ level in the gas phase (blue: negative, red: positive, isovalue: 0.02).

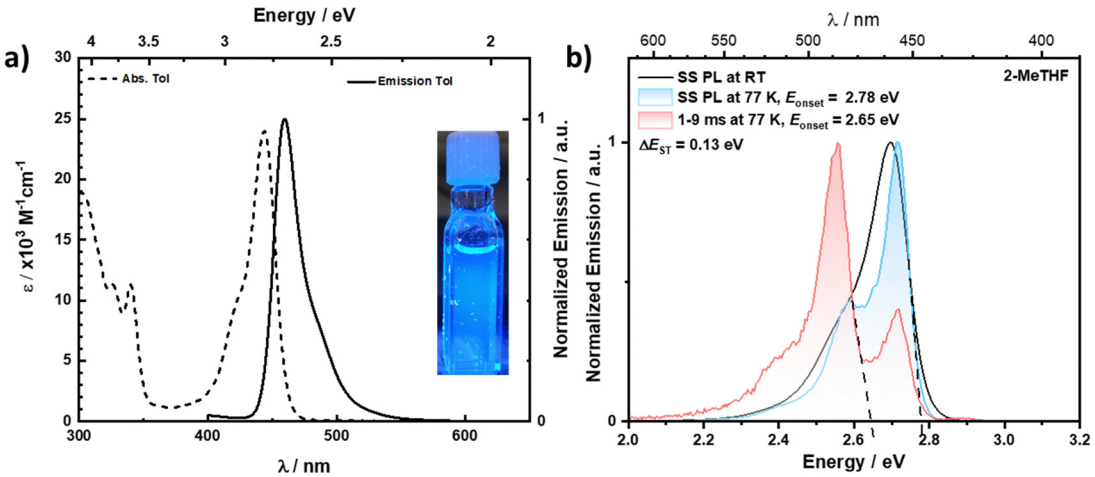

Fig. 3 Absorption and PL spectra of dilute solutions of **Mes-*t*DABNA**; (a) absorption (dashed) and PL spectra (solid) of **Mes-*t*DABNA** in dilute ($\times 10^{-5}$ M) toluene solution (λ_{exc} = 340 nm); (b) steady-state PL spectra of **Mes-*t*DABNA** in dilute 2-MeTHF solution/glass at room temperature (black) and 77 K (blue), time gated (1–9 ms) PL spectrum of **Mes-*t*DABNA** in 2-MeTHF glass (red) (λ_{exc} = 340 nm).

density plots of the S_1 and T_1 states are shown in Fig. 2 (Fig. S1 for **M-*t*DABNA**). Their patterns indicate that both of these states possess SRCT character. The S_0–S_1 transition has a calculated oscillator strength, *f*, of 0.24, which is lower than the corresponding transition in **M-*t*DABNA** (0.28).

Photophysical properties

The absorption and steady-state photoluminescence (PL) spectra in dilute toluene ($\times 10^{-5}$ M) are shown in Fig. 3. The absorption spectrum of **Mes-*t*DABNA** shows an intense lowest energy band at 444 nm with a molar extinction coefficient (ε) of 24×10^3 M^{-1} cm^{-1}. This band is associated with the SRCT transition and is essentially isoenergetic and isoabsorptive as that of ***t*DABNA** (444 nm, 21×10^3 M^{-1} cm^{-1}).[21] The PL spectrum is narrowband with a peak maximum, λ_{PL}, of 460 nm and a full-width at half maximum (FWHM) of 25 nm. This is effectively the same as that of ***t*DABNA** (λ_{PL} of 457 nm and FWHM of 26 nm in toluene).[10] The small Stokes shift of 16 nm is associated with the rigid structure and the small degree of geometric reorganization in the excited state of this compound. The photoluminescence quantum yield, Φ_{PL}, is 75%, which decreases to 54% under aerated conditions. The time-resolved photoluminescence measurements revealed monoexponential decay kinetics, with a prompt lifetime, τ_p, of 7.9 ns, while no delayed emission was observed for **Mes-*t*DABNA** similar to both ***t*DABNA** and **M-*t*DABNA**, and no solution Φ_{PL} or lifetime are reported in the literature. The S_1 and T_1 levels were determined from the onsets of the steady-state and time-gated PL spectra in dilute -methyltetrahydrofuran (2-MeTHF) glass at 77 K (Fig. 3). The S_1 is 2.78 eV and the T_1 is 2.65 eV, resulting in a ΔE_{ST} of 130 meV, all of which are in good agreement with those predicted by the SCS-ADC(2) calculations (S_1 = 2.91 eV; T_1 = 2.75 eV; ΔE_{ST} = 0.16 eV), and is smaller than those reported for ***t*DABNA** (2.82/2.62 eV, ΔE_{ST} = 200 meV in toluene/frozen THF).[10] Compared to **M-*t*DABNA** (ΔE_{ST} = 110 meV in toluene)[15] the ΔE_{ST} is larger by 20 meV, which again is in good agreement with the trend predicted by the SCS-ADC(2) calculations (Fig. 2 and Fig. S1).

The n-type material **SF3-TRZ** was chosen as the host for our emitter due to its suitably high T_1 energy (2.80 eV) and balanced

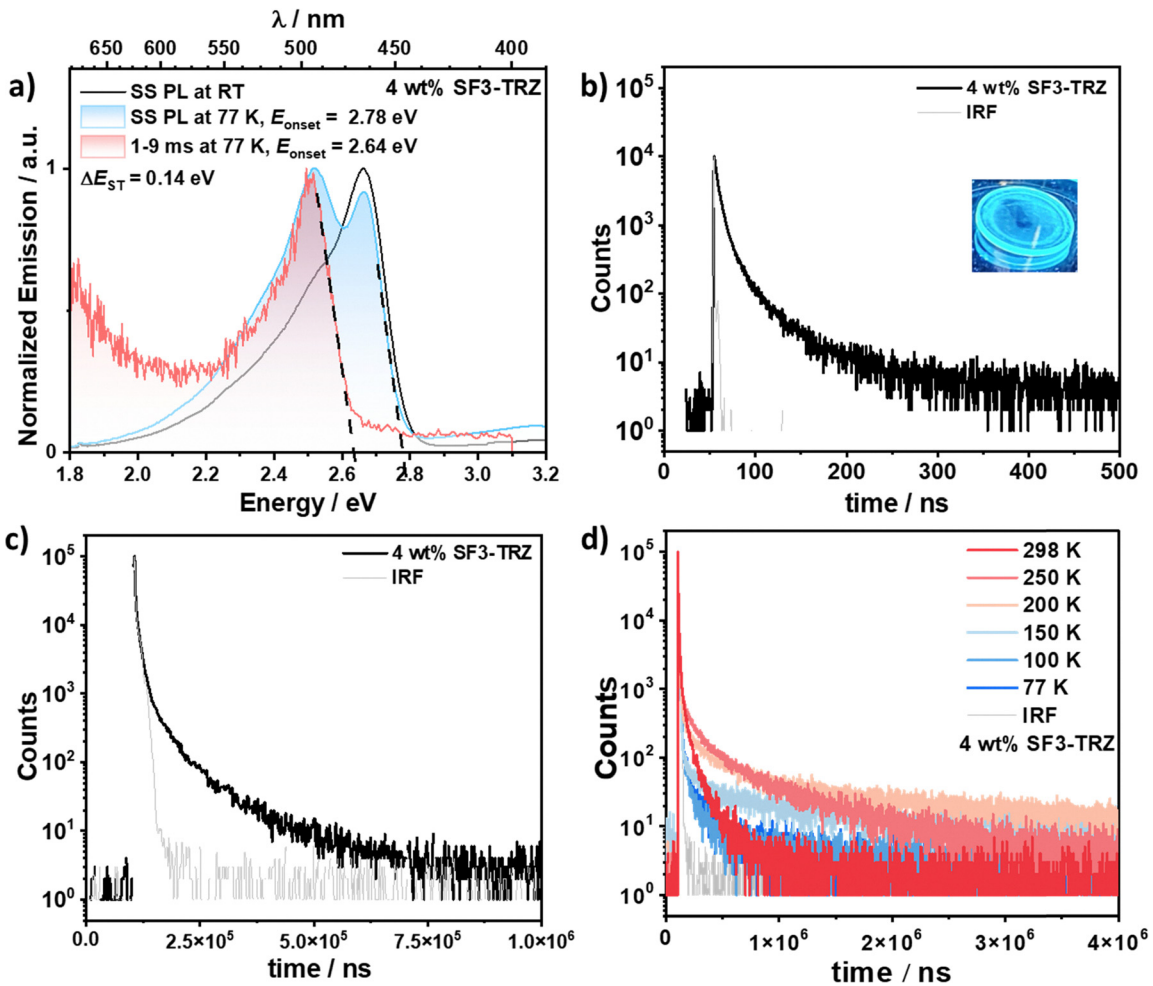

Fig. 4 Photophysical data of the 4 wt% doped film of **Mes-*t*DABNA** in SF3-TRZ; (a) steady-state PL spectra at room temperature (black) and 77 K (blue) and time-gated emission spectrum (1–9 ms) at 77 K (red) (λ_{exc} = 340 nm); (b) time-resolved PL decay under vacuum measured by TCSPC (λ_{exc} = 375 nm); (c) time-resolved PL decay under vacuum measured by MCS (λ_{exc} = 375 nm); (d) temperature-dependent time-resolved PL decay (λ_{exc} = 375 nm).

carrier transporting abilities.[5,22] Excitation at 340 nm into the host of the 4 wt% doped film resulted in efficient Förster resonance energy transfer (FRET) and a Φ_{PL} of 58% (Fig. S6); in air the Φ_{PL} decreases to 20%. In this film **Mes-*t*DABNA** emits at λ_{PL} of 464 nm, with a slightly broader envelope (FWHM of 39 nm), which may indicate that aggregates in the solid state contribute to the emission profile (Fig. 4). The time-resolved PL measurements using time correlated single photon counting (TCSPC) revealed an average $\tau_{p,avg}$ of 13.4 ns (fitted using a multiexponential decay function) and a long emission tail. This delayed emission decay was measured using multichannel scaling (MCS), with an average delayed emission lifetime, $\tau_{d,avg}$, of 45.2 μs. Temperature-dependent time-resolved PL measurements revealed a very weak temperature dependence of the prompt fluorescence decay and a strong temperature dependence of the delayed fluorescence decay, the latter of which confirmed the TADF character of this compound (Fig. 4 and Fig. S8). Additionally, the temperature-dependent PL spectra revealed the emergence of a second emission band at λ_{PL} of 491 nm as the temperature decreased below 150 K, which can be ascribed to phosphorescence (Fig. S9). A ΔE_{ST} of 140 meV was determined from the difference in the onsets of the steady-state PL and the phosphorescence spectra at 77 K. The corresponding S_1 (2.78 eV) and T_1 (2.64 eV) state energies coincide with those measured in 2-MeTHF glass. The rate constants for radiative decay (k_R) and non-radiative decay (k_{NR}) were determined to be 1.46×10^7 and 1.49×10^7 s^{-1}, respectively. The intersystem crossing rate constant for the transition between S_1 and T_1 (k_{ISC}) is 4.47×10^7 s^{-1}, while the reverse intersystem crossing rate constant (k_{RISC}) for the transition from the T_1 level to S_1 level is 5.53×10^4 s^{-1}, a value that is faster than that of ***t*-DABNA** (2.15×10^4 s^{-1} as a 3 wt% doped films in mCBP[10]). A summary of photophysical data is provided in Table 1.

Electrochemistry

Cyclic voltammetry (CV) and differential pulse voltammetry (DPV) measurements in degassed dichloromethane (DCM) containing 0.1 M [^{n}Bu$_4$N]PF$_6$ as a supporting electrolyte and Fc/Fc$^+$ as the internal reference (0.46 V *vs.* saturated calomel electrode (SCE)[25]) were used to determine the HOMO and LUMO energies (Fig. S2). The oxidation wave is irreversible, with an E_{ox} of 0.72 V *vs.* SCE. The corresponding HOMO level is −5.07 eV. This is similar to the HOMO levels reported for **3tPAB** (−5.09 eV) and ***t*DPAC-BN** (−5.10 eV).[13,14] No reduction could be detected, indicating a shallow LUMO level. Therefore, the LUMO level was inferred from the E_{ox} and the optical bandgap, itself determined to be 2.74 eV from the intersection of the normalized absorption and emission spectra in dilute toluene solution (Fig. S13). The corresponding LUMO level is −2.33 eV, which also aligns with the reported measured values for **3tPAB** (−2.36 eV) and ***t*DPAC-BN** (−2.37 eV) in DCM.[13,14] However there are varying HOMO and LUMO levels for DABNA-based emitters reported in the literature. For ***t*DABNA**, **M-*t*DABNA** and ***t*-DABNA-dtB** the reported HOMO/LUMO level are −5.72/−3.02, −5.70/−3.00 and −5.71/−3.08, respectively.[9,10,15] The origin of this difference remains unclear, given that there are only minor structural differences across these three emitters; a possible explanation for the divergence in HOMO/LUMO values could be the application of different conversion equations to derive the energy levels from experimental data.

OLEDs

We next fabricated vacuum-deposited OLEDs with **Mes-*t*DABNA** as the emitter using a device structure consisting of indium tin oxide (ITO)/1,4,5,8,9,11-hexaazatriphenylenehexacarbonitrile (HATCN, 5 nm)/1,1-bis[(di-4-tolylamino)phenyl]cyclohexane (TAPC, 30 nm)/tris(4-carbazoyl-9-ylphenyl)amine (TCTA, 10 nm)/*m*CP (5 nm)/emitting layer (EML) (20 nm)/1,3,5-tris(3-pyridyl-3-phenyl) benzene (TmPyPB, 40 nm)/lithium fluoride (LiF, 1 nm)/aluminum (Al, 100 nm). Here, HATCN was used as the hole injection layer, TAPC and TCTA as the hole transporting layers, *m*CP as an exciton blocking layer, TmPyPB as an electron transporting layer, and LiF was used to reduce the work function of the top Al electrode. The OLED device stack and the chemical structures of the organic layers are shown in Fig. 5d.

We first optimized the doping concentration in SF3-TRZ as a function of Φ_{PL} (Fig. S6). A doping concentration of 4 wt% provided charge balance and a sufficiently large exciton recombination zone, and the Φ_{PL} remained high at this concentration (*vide supra*) and an EQE_{max} of 18.4% was achieved at this doping concentration. The electroluminescence (EL) spectrum, current density–voltage-luminance (*J*–*V*–*L*) curves and EQE *vs.* luminescence curves are shown in Fig. 5a–c. The device with **Mes-*t*DABNA** emitted narrowband blue light at λ_{EL} of 468 nm (FWHM of 32 nm), which corresponds to CIE coordinates of

Table 1 Photophysical data of **Mes-*t*DABNA** in dilute solution and doped film

Compound	$\lambda_{Abs}(\varepsilon)^a$/nm ($\times 10^3$ M^{-1} cm^{-1})	$\lambda_{PL}{}^{ab}$/nm	FWHM^{ab}/nm	$E_{S1}{}^{cd}$/eV	$E_{T1}{}^{ef}$/eV	$\Delta E_{ST}{}^g$/eV	$\Phi_{PL}{}^{hi}$/%	$\tau_{p,avg}{}^j$/ns	$\tau_{d,avg}{}^k$/μs	$k_{ISC}{}^l$/$\times 10^7$ s^{-1}	$k_{RISC}{}^l$/$\times 10^4$ s^{-1}	$k_{s\_r}{}^l$/$\times 10^7$ s^{-1}
Mes-*t*DABNA	444 (24)	460/464	25/39	2.78/2.78	2.65/2.64	0.13/0.14	58/75	7.9/13.4	—/45.2	4.47	5.53	1.49

[a] In toluene solution (10^{-5} M). [b] Measured as spin-coated thin films consisting of 4 wt% emitter in SF3-TRZ host. λ_{exc} = 340 nm. [c] Onset of steady-state emission at 77 K in 2-MeTHF glass λ_{exc} = 340 nm. [d] Onset of the SS PL at 77 K in 4 wt% doped film in SF3-TRZ. λ_{exc} = 340 nm. [e] Onset of the time-gated PL spectrum (1–9 ms) at 77 K in 2-MeTHF glass. λ_{exc} = 340 nm. [f] Onset of the time-gated PL spectrum (1–9 ms) at 77 K in 4 wt% doped film in SF3-TRZ. λ_{exc} = 340 nm. [g] $\Delta E_{ST} = E(S_1) - E(T_1)$. [h] Absolute Φ_{PL} of the thin films measured using an integrating sphere. λ_{exc} = 340 nm. [i] Φ_{PL} in solution was measured by the relative method using quinine sulfate as the reference (Φ_r = 54.6% in 1 N H_2SO_4).[23] [j] Prompt PL lifetimes were measured by TCSPC and fitting the decay to a multiexponential decay function λ_{exc} = 375 nm. [k] Delayed PL lifetimes were measured by MCS and fitting the decay to a multiexponential decay function λ_{exc} = 375 nm. [l] Intersystem and reverse intersystem crossing rate constants were calculated using the steady-state approximation method as described in the literature.[24]

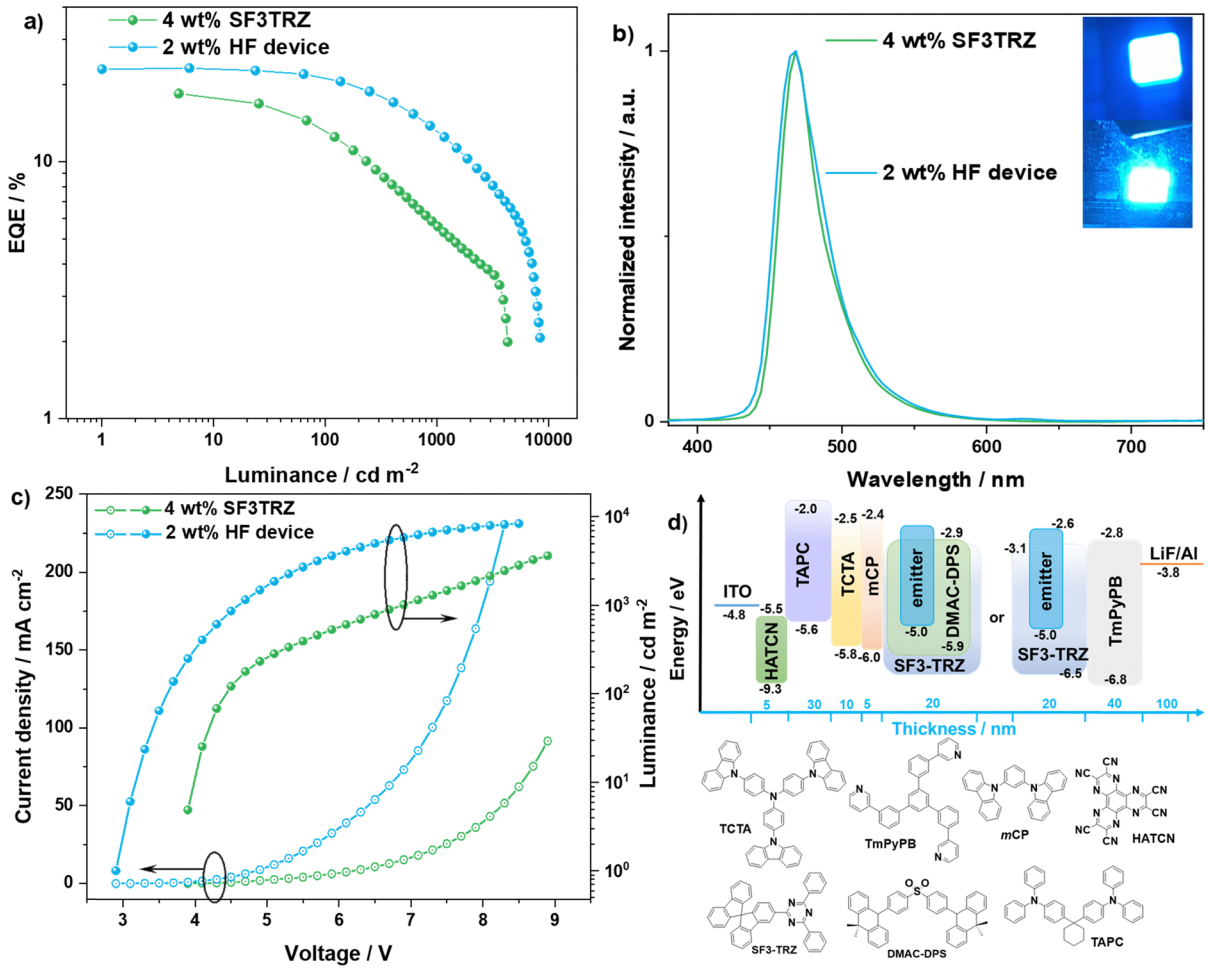

Fig. 5 Device data of **Mes-*t*DABNA** (green = conventional device) (blue = HF device) (a) EQE *vs.* luminance plot; (b) electroluminescence spectra; (c) *J*–*V*–*L* plot (d) device structure and chemical structures of used materials.

(0.13, 0.15). These are identical to the reported device with ***t*DABNA** in DPEPO.[9] Compared to the devices with ***t*-DABNA-dtB** (λ_{EL} = 471 nm), the λ_{EL} is blue-shifted; however, due to the broader envelope of the EL spectrum of the device with **Mes-*t*DABNA** the CIE_y coordinate is increased from 0.13 for the device with ***t*-DABNA-dtB** (FWHM = 140 meV) to 0.15 for the device with **Mes-*t*DABNA** (FWHM = 190 meV). The EL spectrum is narrower than the corresponding PL spectrum (Fig. 4), which is likely due to the more homogeneous film achieved by vacuum deposition compared to the spin-coated film used for the PL measurements. The device with **Mes-*t*DABNA** showed an EQE_{max} of 18.4% and a maximum brightness, L_{max}, of 3600 cd m^{-2}. Due in part to its relatively slow k_{RISC}, the device showed relatively severe efficiency roll-off at high luminance (EQE_{100} and EQE_{1000} of 12.5 and 5.6%, respectively); however, the efficiency roll-off was nonetheless milder compared to devices with **DABNA-1** and ***t*DABNA**, as neither were reported to reach 1000 cd m^{-2}.[8,9] The device with **Mes-*t*DABNA** performed comparably to one of the best devices with the DABNA derivative **DABNA-NP-TB**, which has a reported EQE_{max}/EQE_{1000} of 19.5/12.0% (Fig. 6 and Table S3).[12]

In a bid to improve the exciton utilization efficiency and reduce the efficiency roll-off, HF OLEDs were fabricated (Fig. 5d). **DMAC-DPS** was used as the TADF assistant dopant because of its high Φ_{PL} of 90%, relatively fast k_{RISC} of 2.9×10^5 s^{-1} in 20 wt% doped SF3-TRZ film, and the strong overlap between the absorption spectrum of **Mes-*t*DABNA** and the PL spectrum of **DMAC-DPS** in toluene (Fig. S13). An optimized doping ratio of 2 wt% **Mes-*t*DABNA**: 20 wt% **DMAC-DPS**: 78 wt% SF3-TRZ was identified to be used as the EML as this formulation minimized the probability for triplet excitons from the host to transfer to the **Mes-*t*DABNA** and permitted an efficient FRET from **DMAC-DPS** to **Mes-*t*DABNA**, thereby conserving the narrowband emission (Table 2 and Fig. S10). The photophysical properties of the hyperfluorescent film are compiled in Table S2. As shown in Fig. 5b, the HF devices showed similar narrowband emission at λ_{EL} of 469 nm (FWHMs of 34 nm) and CIE coordinates of (0.13, 0.17) to the conventional device. The turn-on voltages (V_{on}) were reduced from 3.9 to 3.1 V and the EQE_{max} was improved to 23.1%. More importantly, the efficiency roll-off was reduced, with EQE_{100} and EQE_{1000} of 20.5 and 12.7%, respectively. Compared to the HF devices with the derivatives ***t*DPAC-BN** (EQE_{max}/EQE_{1000} = 21.0/5.4%) and **M-*t*DABNA**

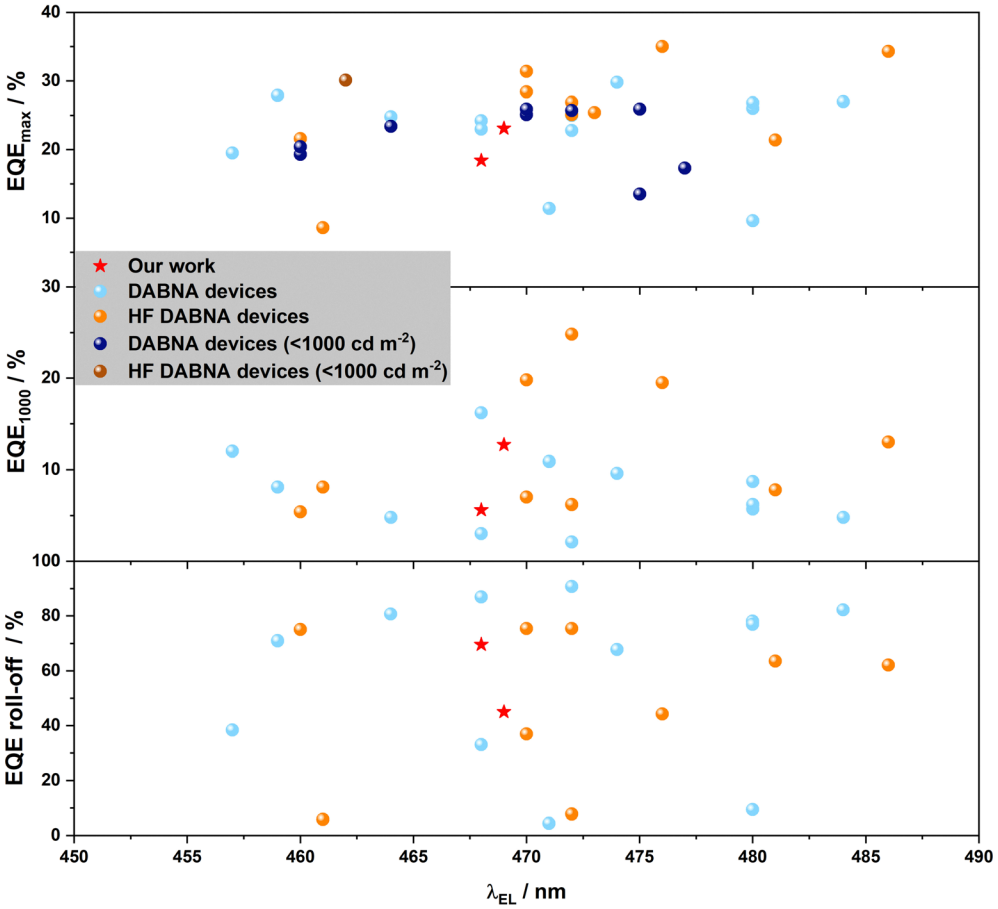

Fig. 6 EQE$_{max}$, EQE$_{1000}$ and EQE roll-off *vs.* λ_{EL} of devices employing DABNA-based emitters in the literature; EQE roll-off refers to the efficiency roll-off from EQE$_{max}$ to EQE$_{1000}$. Light blue points represent conventional devices; orange points represent HF devices; dark blue points represent conventional devices that did not reach a L_{max} of 1000 cd m^{-2}; brown points represent HF device that did not reach a L_{max} of 1000 cd m^{-2}; data presented are listed in Table S2.

Table 2 Device data of **Mes-*t*DABNA**

Conventional device[a]	V_{on}/V	λ_{EL}[c] (FWHM)/nm	L_{max}/cd m^{-2}	EQE$_{max/100/1000}$/%	CIE (x, y)[c]
Mes-*t*DABNA (4 wt%)	3.9	468 (33)	3600	18.4/12.5/5.6	0.13, 0.15
HF device[b]					
Mes-*t*DABNA (2 wt%)	3.3	469 (34)	8400	23.1/20.5/12.7	0.13, 0.17

[a] Using an EML consisting of 4 wt% **Mes-*t*DABNA** in SF3-TRZ. [b] Using an EML consisting of **Mes-*t*DABNA**:**DMAC-DPS**:SF3-TRZ = 2 : 20 : 78 wt%.

(EQE$_{max}$/EQE$_{1000}$ = 8.6/8.1%), the OLED with **Mes-*t*DABNA** showed an enhanced performance evidenced by the milder efficiency roll-off (see additional device comparison data in Table S3 in the SI).

Conclusions

Here, we demonstrated an effective substitution strategy to mitigate aggregation-caused quenching in thin films while preserving narrowband blue emission in a DABNA derivative MR-TADF emitter. This approach also resulted in devices showing milder efficiency roll-off and higher EQE$_{max}$, attributed to a smaller ΔE_{ST}, shorter delayed lifetime, and a faster k_{RISC}, compared to devices with ***t*DABNA**. **Mes-*t*DABNA** emits at λ_{PL} at 460 nm and has a narrow emission envelope with a FWHM of 25 nm. The devices showed an EQE$_{max}$ of 18.4% at blue CIE coordinates (0.13, 0.15); however though improved over devices with ***t*DABNA** there remained a significantly efficiency roll-off (EQE$_{1000}$ of 5.6%, compared to 0.4% for the device with ***t*DABNA**). To further improve the device performance, the D–A type TADF emitter, **DMAC-DPS**, was employed as a sensitizer within a HF device configuration, resulting in a higher EQE$_{max}$ of 23.1% and lower efficiency roll-off (EQE$_{1000}$ of 12.7%) compared to the traditional device. In contrast, most ***t*DABNA**-based emitters in HF devices exhibit EQE$_{1000}$ values below 10%. These results underscore the critical role of molecular design in tailoring photophysical properties to enhance device performance.

Author contributions

M. F.: conceptualization, data curation, formal analysis, investigation, methodology, visualization, writing – original draft preparation, writing – review & editing. D. C.: data curation, formal analysis, investigation, visualization, writing – original draft preparation, writing – review & editing. E. Z.-C.: conceptualization, funding acquisition, methodology, project administration, resources, supervision, writing – review & editing.

Conflicts of interest

There are no conflicts to declare.

Data availability

The research data supporting this publication can be accessed at **https://doi.org/10.17630/e4521ae2-e1ea-45c2-8f60-880c6d12e8a6**.

Supplementary information: ^{1}H NMR and ^{13}C NMR spectra, HRMS, elemental analysis and reverse phase HPLC; supplementary computational data and coordinates; additional photophysical and OLED data. See DOI: **https://doi.org/10.1039/d5ma00586h**

Acknowledgements

This project has been partly funded by the European Union Horizon 2021 research and innovation programme under grant agreement no. 101073045 (TADF solutions) and the EPSRC grant EP/X026175/1. In the UK, this project has received funding from the Engineering and Physical Sciences Research Council for support (EP/R035164/1; EP/W007517/1; EP/Z535291/1). D. Chen thanks the support from China Postdoctoral Science Foundation (Grant no. 2022TQ0227) and Natural Science Foundation of Jiangsu Province, China (Grant no. BK20230508). We thank Prof. Xiao-Hong Zhang for providing access to the device fabrication facility at Soochow University.

References

1 H. Uoyama, K. Goushi, K. Shizu, H. Nomura and C. Adachi, *Nature*, 2012, **492**, 234–238.
2 S. Madayanad Suresh, D. Hall, D. Beljonne, Y. Olivier and E. Zysman-Colman, *Adv. Funct. Mater.*, 2020, **30**, 1908677.
3 R. K. Konidena and K. R. Naveen, *Adv. Photon. Res.*, 2022, **3**, 2200201.
4 K. R. Naveen, P. Palanisamy, M. Y. Chae and J. H. Kwon, *Chem. Commun.*, 2023, **59**, 3685–3702.
5 X.-C. Fan, K. Wang, Y.-Z. Shi, Y.-C. Cheng, Y.-T. Lee, J. Yu, X.-K. Chen, C. Adachi and X.-H. Zhang, *Nat. Photonics*, 2023, **17**, 280–285.
6 Y. C. Cheng, X. Tang, K. Wang, X. Xiong, X. C. Fan, S. Luo, R. Walia, Y. Xie, T. Zhang, D. Zhang, J. Yu, X. K. Chen, C. Adachi and X. H. Zhang, *Nat. Commun.*, 2024, **15**, 731.
7 H. Wang, Y. C. Cheng, X. C. Fan, D. Y. Chen, X. Xiong, X. Y. Hao, Y. Z. Shi, J. Yu, D. Huang, J. X. Chen, K. Wang and X. H. Zhang, *Sci. Bull.*, 2024, **69**, 2983–2986.
8 T. Hatakeyama, K. Shiren, K. Nakajima, S. Nomura, S. Nakatsuka, K. Kinoshita, J. Ni, Y. Ono and T. Ikuta, *Adv. Mater.*, 2016, **28**, 2777–2781.
9 S. H. Han, J. H. Jeong, J. W. Yoo and J. Y. Lee, *J. Mater. Chem. C*, 2019, **7**, 3082–3089.
10 J. Park, K. J. Kim, J. Lim, T. Kim and J. Y. Lee, *Adv. Mater.*, 2022, **34**, e2108581.
11 J. H. Kim, W. J. Chung, J. Kim and J. Y. Lee, *Mater. Today Energy*, 2021, **21**, 100792.
12 S. Oda, W. Kumano, T. Hama, R. Kawasumi, K. Yoshiura and T. Hatakeyama, *Angew. Chem., Int. Ed.*, 2021, **60**, 2882–2886.
13 Y. Wang, Y. Duan, R. Guo, S. Ye, K. Di, W. Zhang, S. Zhuang and L. Wang, *Org. Electron.*, 2021, **97**, 106275.
14 Y. Wang, K. Di, Y. Duan, R. Guo, L. Lian, W. Zhang and L. Wang, *Chem. Eng. J.*, 2022, **431**, 133221.
15 H. Lim, S. J. Woo, Y. H. Ha, Y. H. Kim and J. J. Kim, *Adv. Mater.*, 2022, **34**, e2100161.
16 Y. Yuan, X. Tang, X. Y. Du, Y. Hu, Y. J. Yu, Z. Q. Jiang, L. S. Liao and S. T. Lee, *Adv. Opt. Mater.*, 2019, **7**, 1801536.
17 D. Hall, S. M. Suresh, P. L. dos Santos, E. Duda, S. Bagnich, A. Pershin, P. Rajamalli, D. B. Cordes, A. M. Z. Slawin, D. Beljonne, A. Köhler, I. D. W. Samuel, Y. Olivier and E. Zysman-Colman, *Adv. Opt. Mater.*, 2019, **8**, 1901627.
18 D. Hall, J. C. Sancho-Garcia, A. Pershin, D. Beljonne, E. Zysman-Colman and Y. Olivier, *J. Phys. Chem. A*, 2023, **127**, 4743–4757.
19 P. Ulukan, A. Monari and S. Catak, *ChemPhotoChem*, 2023, **7**, e202300147.
20 D. Hall, J. C. Sancho-Garcia, A. Pershin, G. Ricci, D. Beljonne, E. Zysman-Colman and Y. Olivier, *J. Chem. Theory Comput.*, 2022, **18**, 4903–4918.
21 L. Hämmerling and E. Zysman-Colman, *Chem. Catal.*, 2024, **4**, 101061.
22 L. S. Cui, S. B. Ruan, F. Bencheikh, R. Nagata, L. Zhang, K. Inada, H. Nakanotani, L. S. Liao and C. Adachi, *Nat. Commun.*, 2017, **8**, 2250.
23 W. H. Melhuish, *J. Phys. Chem.*, 1961, **65**, 229.
24 Y. Tsuchiya, S. Diesing, F. Bencheikh, Y. Wada, P. L. dos Santos, H. Kaji, E. Zysman-Colman, I. D. W. Samuel and C. Adachi, *J. Phys. Chem. A*, 2021, **125**, 8074.
25 V. V. Pavlishchuk and A. W. Addison, *Inorg. Chim. Acta*, 2000, **298**, 97–102.